Chapter 10
Modeling of Airborne Wind Energy Systems in Natural Coordinates

Sébastien Gros, Moritz Diehl

Abstract This paper presents a modeling approach for AWE systems that allows for developing models of low symbolic complexity and low nonlinearity. The approach is based on multi-body modeling, using natural coordinates and algebraic constraints as a representation of the system evolution. This paper shows how to build such models for AWE systems in the Lagrangian framework and how to efficiently incorporate a non-singular representation of the pose (i.e. 3D orientation) of the wing. The proposed modeling technique is illustrated on a single-wing AWE system for power generation and rotating start-up, and for a dual-wing AWE system.

10.1 Introduction

Modeling is a crucial element of Airborne Wind Energy (AWE) for system simulation, optimization, and control. AWE systems are intricate mechanical systems, where the winch, tether(s), and wing(s) interact dynamically to yield complex, fast and nonlinear dynamics. Control models for AWE systems have been presented in the literature [3–5, 10, 16, 17, 19], and commonly assume that the wing evolves on a sphere centered at the lower attachment point of the tether. A high-fidelity simulation models for inflatable kites based on a multi-body approach is presented in [6]. Most models are based on a minimal coordinates formulation, where e.g. the evolution of the wing on a sphere is embedded in the model equations using spherical coordinates. The pose of the wing, i.e. its 3D orientation in space, is often represented using standard Euler angles, or quaternions.

Though the minimal coordinate approach is an intuitive modeling choice, it also has several drawbacks: 1) because the Riemannian metric in spherical coordinates is nonlinear and non-diagonal, and appears implicitly throughout the dynamics, the

Sébastien Gros (✉) · Moritz Diehl
KU Leuven, Electrical Engineering Department, Arenberg Kasteelpark 10, 3001 Leuven, Belgium,
e-mail: grosse@chalmers.se

model symbolics become intricate, 2) computing the projection of the wing relative velocity into its reference frame involves elaborate nonlinear transformations, 3) the representation of the pose of the wing based on Euler angles has singularities, which adds extra difficulties for AWE systems where all wing configurations are likely to be visited. Thereby, models based on minimal coordinates, though they are rather simple to formulate mathematically, are strongly nonlinear and complex. This difficulty is especially salient for multiple-wing AWE systems, where multiple reference frames need to be used.

It has been observed in multi-body modeling that the model efficiency and simplicity can be significantly improved by considering each body separately and by linking them through algebraic constraints [15]. A similar approach is presented here to develop models for AWE systems.

Non-minimal coordinates yield model equations in the form of index-3 DAEs, where the constraints represent the links between the various bodies. In the context of optimal control, high-index DAEs are best treated using index-reduction techniques [12], where the constraints are differentiated with respect to time so as to obtain index-1 DAEs with associated consistency conditions. The index-reduced DAEs describing the dynamics of multi-body systems usually retain a very reasonable symbolic complexity. This paper presents a technique to develop the index-1 DAEs directly from the set of Lagrange functions [13] and algebraic constraints describing the multi-body systems.

The most popular non-singular parametrization of the $SO(3)$ special orthogonal Lie group, i.e. the group used to represent the orientation of an object in space (see e.g. [11] for further details) is based on the four-dimensional unitary quaternion vector. In the context of optimal control, however, early results suggest that a Direct Cosine Matrix (DCM) or rotationless formulation of the $SO(3)$ representation can be better suited because it reduces the nonlinearity of the model equations. The DCM formulation, however, requires a larger number of states than a quaternion-based parametrization. This paper presents a systematic projection technique to reduce the number of states needed in the model. The lower complexity and lower nonlinearity of the models resulting from the proposed modeling approach are well suited for Newton-type optimization techniques, and fast optimization-based control techniques.

The paper is organized as follows. Section 10.2 provides preliminaries on the Lagrangian modeling in natural coordinates, and describes a technique to include the DCM in the Lagrangian formalism. Section 10.3 presents a model for a single-wing AWE system in natural coordinates, Sect. 10.4 describes a model for a dual-wing AWE system in natural coordinates. Section 10.5 presents a model for a rotational startup of AWE systems, using reference frames attached to the carousels. Section 10.6 presents simple techniques to deal with the issue of stabilizing the constraints resulting from the Natural Coordinate modeling approach. Section 10.7 presents an illustrative simulation of the carousel model presented in Sect. 10.5. Section 10.8 presents a comparison of the modeling of a dual-wing system using both the minimal and natural coordinate approach in term of computational cost and complexity followed by conclusion presented in Sect. 10.9.

10.2 Natural coordinates in Lagrangian Mechanics

In Lagrangian mechanics [13], the configuration of a system is described by an arbitrary, independent set of generalized coordinates $\mathbf{q} \in Q$ restricted to evolve on a given manifold $c(\mathbf{q}) = 0$ with $c : Q \to C$. The Lagrange function of the system is defined as [13]:

$$\mathscr{L}(\mathbf{q}, \dot{\mathbf{q}}, \nu) = T(\mathbf{q}, \dot{\mathbf{q}}) - V(\mathbf{q}) - \langle \nu, c(\mathbf{q}) \rangle, \tag{10.1}$$

where T and V stand for the kinetic and potential energy of the system, respectively, ν is the set of Lagrange multipliers associated to the constraints c, and $\langle ., . \rangle$ is the scalar product on C. Observe that Q and C are not necessarily $\mathbb{R}^\bullet$, but can e.g. mix vector and matrices (see Sect. 10.2.2). The motion of the system, i.e. the time trajectory $\mathbf{q}(t)$ of its generalized coordinates is defined by the Lagrange equations:

$$\frac{\mathrm{d}}{\mathrm{d}t} \frac{\partial \mathscr{L}}{\partial \dot{\mathbf{q}}} - \frac{\partial \mathscr{L}}{\partial \mathbf{q}} = \mathbf{F}_\mathbf{q}, \quad c(\mathbf{q}) = 0. \tag{10.2}$$

where $\mathbf{F}_\mathbf{q}$ is the vector of generalized forces acting on the system. The generalized forces $\mathbf{F}_\mathbf{q}$ are defined by the *virtual work* condition: for any infinitesimal displacement $\delta\mathbf{q}$ of the system configuration, yielding the work δW on the system, the equality:

$$\delta W = \langle \delta\mathbf{q}, \mathbf{F}_\mathbf{q} \rangle \tag{10.3}$$

must hold, where $\langle ., . \rangle$ is the scalar product on Q.

Equation (10.2) is an index-3 Differential Algebraic Equation (DAE). Because the algebraic variables ν do not appear explicitly in the constraint c, it is difficult to integrate (Eq. 10.2) [2]. A better form can be obtained by index reduction. The constraint $c(\mathbf{q})$ is differentiated twice with respect to time, such that the generalized accelerations $\ddot{\mathbf{q}}$ appear:

$$\dot{c}_i = \dot{\mathbf{q}}^T \nabla_\mathbf{q} c_i, \quad \ddot{c}_i = \dot{\mathbf{q}}^T \nabla_\mathbf{q} \dot{c}_i + \ddot{\mathbf{q}}^T \nabla_{\dot{\mathbf{q}}} \dot{c}_i \tag{10.4}$$

where ∇_A is the differential operator with respect to the element of $A \in \mathbb{R}^{n \times m}$ on single-valued functions, preserving the structure of A, i.e.

$$\nabla_A = \begin{bmatrix} \frac{\partial}{\partial A_{11}} & \cdots & \frac{\partial}{\partial A_{1m}} \\ & \cdots & \\ \frac{\partial}{\partial A_{n1}} & \cdots & \frac{\partial}{\partial A_{nm}} \end{bmatrix} \tag{10.5}$$

In the simple case that $\mathbf{q}$ is a vector, $\nabla_\mathbf{q}$ is the classical derivative operator, i.e. $\nabla_\mathbf{q} = \begin{bmatrix} \frac{\partial}{\partial q_1} & \cdots & \frac{\partial}{\partial q_n} \end{bmatrix}^T$. The very same definition pertains to operator $\nabla_{\dot{\mathbf{q}}}$, where the differentiation is performed with respect to $\dot{\mathbf{q}}$. The system dynamics are then given

by:

$$\frac{\mathrm{d}}{\mathrm{d}t}\frac{\partial \mathscr{L}}{\partial \dot{\mathbf{q}}} - \frac{\partial \mathscr{L}}{\partial \mathbf{q}} = \mathbf{F}_{\mathbf{q}}, \quad \ddot{c}_i = 0 \tag{10.6}$$

It can be verified that equations (10.6) are linear in $\ddot{\mathbf{q}}$ and v. In addition to (Eq. 10.6), the *consistency conditions*

$$c_i(t_c) = 0, \qquad \dot{c}_i(t_c) = 0 \tag{10.7}$$

must be satisfied at any arbitrary time t_c of the system trajectory to yield a physically consistent system trajectory.

10.2.1 Illustrative Example

Consider a point mass m attached to the origin by a massless rod of length l (see Fig. 10.1, left), subject to gravity and an external force vector $\mathbf{F}$. In natural coordinates, the position of the mass is given by the vector $\mathbf{q} = \begin{bmatrix} x & y & z \end{bmatrix}^T$, and the mass is constrained to evolve on the manifold described by the single constraint

$$c(\mathbf{q}) = \frac{1}{2}\left(\mathbf{q}^T\mathbf{q} - l^2\right) = 0. \tag{10.8}$$

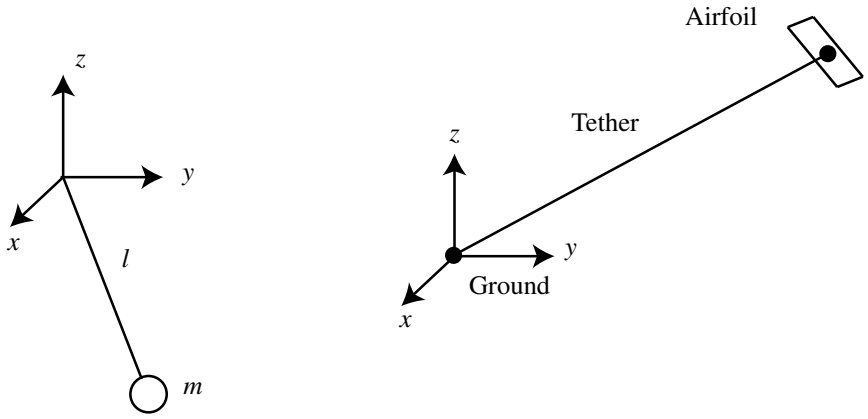

Fig. 10.1 Pendulum Schematic (left figure) and Single kite architecture (right figure)

The Lagrange function of the system is:

$$\mathscr{L}(\mathbf{q},\dot{\mathbf{q}},\nu) = \frac{1}{2}m\dot{\mathbf{q}}^T\dot{\mathbf{q}} - mg\mathbf{1}_z^T\mathbf{q} - \frac{1}{2}\nu\left(\mathbf{q}^T\mathbf{q} - l^2\right) \tag{10.9}$$

where $\mathbf{1}_z^T = [0\ 0\ 1]$. For any displacement $\delta\mathbf{q}$, the amount of work δW performed on the system is given by:

$$\delta W = \delta\mathbf{q}^T\mathbf{F} = \langle\delta\mathbf{q}, \mathbf{F}_\mathbf{q}\rangle \tag{10.10}$$

therefore $\mathbf{F} = \mathbf{F}_\mathbf{q}$. Using (Eq. 10.4), the index-reduction reads:

$$\dot{c}(\mathbf{q},\dot{\mathbf{q}}) = \mathbf{q}^T\dot{\mathbf{q}} - l\dot{l}, \quad \ddot{c}(\mathbf{q},\dot{\mathbf{q}},\ddot{\mathbf{q}}) = \mathbf{q}^T\ddot{\mathbf{q}} + \dot{\mathbf{q}}^T\dot{\mathbf{q}} - \dot{l}^2 - l\ddot{l} \tag{10.11}$$

Using (Eq. 10.6), the dynamics are given by:

$$m\ddot{\mathbf{q}} + \nu\mathbf{q} = \mathbf{F} - mg\mathbf{1}_z, \quad \mathbf{q}^T\ddot{\mathbf{q}} + \dot{\mathbf{q}}^T\dot{\mathbf{q}} - \dot{l}^2 - l\ddot{l} = 0, \tag{10.12}$$

which can be rewritten in the structured form:

$$\begin{bmatrix} mI & \mathbf{q} \\ \mathbf{q}^T & 0 \end{bmatrix}\begin{bmatrix} \ddot{\mathbf{q}} \\ \nu \end{bmatrix} = \begin{bmatrix} \mathbf{F} - mg\mathbf{1}_z \\ -\dot{\mathbf{q}}^T\dot{\mathbf{q}} + \dot{l}^2 + l\ddot{l} \end{bmatrix} \tag{10.13}$$

where I is the identity matrix. The dynamics (Eq. 10.13) represent the motion of the tethered mass if the following consistency conditions are respected by $\mathbf{q},\dot{\mathbf{q}}$ at some time t_c:

$$c = \frac{1}{2}\left(\mathbf{q}^T\mathbf{q} - l^2\right)_{t=t_c} = 0, \quad \dot{c} = \left(\mathbf{q}^T\dot{\mathbf{q}} - l\dot{l}\right)_{t=t_c} = 0. \tag{10.14}$$

It can be observed in (Eq. 10.13) that $\mathbf{q}\nu$ is equivalent to a force. It is in fact the force constraining the mass to evolve on its manifold, i.e. the force in the rod.

10.2.2 Lagrangian Mechanics on the $SO(3)$ Lie group

The $SO(3)$ special orthogonal Lie group is used to represent the 3D orientation of objects in space. The Direct Cosine Matrix (DCM) embeds such orientations in a 3×3 matrix by describing the rotation transforming vectors in the object frame into the fixed frame. In the following, it will be useful to decompose the DCM in its columns $\mathbf{e}_{1,2,3}\in\mathbb{R}^3$, i.e. $R = \begin{bmatrix}\mathbf{e}_1\ \mathbf{e}_2\ \mathbf{e}_3\end{bmatrix}$, such that $\mathbf{e}_{1,2,3}$ are the longitudinal, transversal, and vertical axis of the wing respectively (see Fig. 10.2). The time evolution of the DCM reads

$$\dot{R} = R\omega_\times, \tag{10.15}$$

where $\omega\in\mathbb{R}^3$ is the vector of angular velocity in the wing reference frame e, and $\cdot_\times$ is the skew operator that transforms a vector of $\mathbb{R}^3$ into the corresponding skew-symmetric matrix.

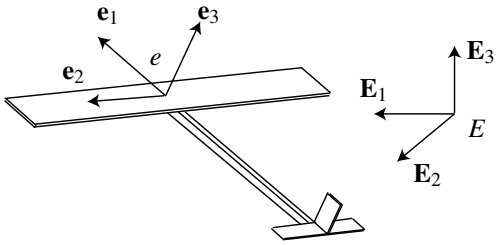

Fig. 10.2 Ground and wing reference frame, E and e respectively.

Consider a 6DOF body described by the set of generalized coordinates $q = \{\mathbf{r}, R\}$ (where q is not a vector per se since it is composed of the matrix R and the vector $\mathbf{r}$), where $\mathbf{r} = [x\ y\ z]^T$ is the position of the center of mass of the body in the fixed frame E and $R \in \mathbb{R}^{3\times 3}$ its Direct Cosine Matrix (DCM), subject to the constraints:

$$c(\mathbf{r}, R) = 0, \quad R^T R - I = 0 \tag{10.16}$$

The Lagrangian reads:

$$\mathscr{L} = T - V - \nu^T c(\mathbf{r}, R) - \mathrm{tr}\left(Z^T \left(R^T R - I\right)\right), \tag{10.17}$$

where $Z \in \mathbb{S}^3$ is the symmetric matrix of Lagrange multipliers associated to the orthonormality constraint $R^T R = I$, $\nu \in \mathbb{R}^{n_c}$ is the Lagrange multiplier associated to the constraints $c = 0$, and the trace operator tr yields the scalar product on matrix vector spaces. Formulation (Eq. 10.2) then reads:

$$\begin{aligned} \frac{\mathrm{d}}{\mathrm{d}t}\nabla_{\dot{\mathbf{r}}}\mathscr{L} - \nabla_{\mathbf{r}}\mathscr{L} &= \mathbf{F}_{\mathbf{r}}, \quad c(\mathbf{r}, R) = 0 \\ \frac{\mathrm{d}}{\mathrm{d}t}\nabla_{\dot{R}}\mathscr{L} - \nabla_{R}\mathscr{L} &= F_R, \quad R^T R - I = 0 \end{aligned} \tag{10.18}$$

Note that the rotational part in (Eq. 10.18) are 3×3 differential equations defining $\ddot{R} \in \mathbb{R}^{3\times 3}$. The dimension of that equation can be reduced to 3 using the fact that

$$\ddot{R} = R\dot{\omega}_{\times} - \dot{R}R^T\dot{R} \tag{10.19}$$

so that $\ddot{R}$ can be parametrized by only 3 variables instead of 9. Additionally, the rotational kinetic energy is typically developed based on the angular velocity ω rather than the time derivative of the rotation matrix $\dot{R}$, i.e.

$$T = \frac{1}{2}\omega^T J \omega + \frac{1}{2} m \dot{\mathbf{r}}^T \dot{\mathbf{r}} \tag{10.20}$$

where J is the matrix representation of the object inertia tensor given in the object reference frame e, and m its mass. In the following, a reduction technique is presented to obtain a set of 3 equations defining the angular accelerations $\dot{\omega}$ instead of $\ddot{R}$. To that end, we introduce a fundamental operator. Defining U as the "unskew"

operator:

$$U\left(\begin{bmatrix} a_{11} & a_{12} & a_{13} \\ a_{21} & a_{22} & a_{23} \\ a_{31} & a_{32} & a_{33} \end{bmatrix}\right) = \frac{1}{2}\begin{bmatrix} a_{32}-a_{23} \\ a_{13}-a_{31} \\ a_{21}-a_{12} \end{bmatrix}, \quad U(\mathbf{a}_\times) = \mathbf{a}, \tag{10.21}$$

The linear operator $P_R : \mathbb{R}^{3\times 3} \to \mathbb{R}^3$ is then defined as

$$P_R(A) = U\left(R^T A\right), \tag{10.22}$$

and relates differentials over $SO(3)$ to their $\mathbb{R}^3$ counterparts, i.e. $\mathrm{d}\omega = P(\delta R) \in \mathbb{R}^3$ such that $\delta R = R\mathrm{d}\omega_\times$. As a result, the following equalities hold:

$$P_R(\dot{R}) = U(R^T\dot{R}) = U(R^T R\omega_\times) = \omega, \quad \dot{R} = R\omega_\times \tag{10.23}$$

It can be shown that the gradient of the orthonormality constraints reads:

$$\nabla_R \mathrm{tr}\left(Z(R^T R - I)\right) = R\left(Z + Z^T\right). \tag{10.24}$$

Because $R^T\nabla_R \mathrm{tr}\left(Z(R^T R - I)\right) = R^T R\left(Z + Z^T\right) = \left(Z + Z^T\right)$ is symmetric, it follows that

$$P_R\left(\nabla_R \mathrm{tr}\left(Z(R^T R - I)\right)\right) = 0 \tag{10.25}$$

Some properties of operators U and P are presented in the Appendix.

Proposition 10.1. *The following equality holds:*

$$2P_R\left(\frac{\mathrm{d}}{\mathrm{d}t}\nabla_{\dot{R}}\left(\frac{1}{2}\omega^T J\omega\right) - \nabla_R\left(\frac{1}{2}\omega^T J\omega\right)\right) = J\dot{\omega} + \omega\times J\omega, \quad 2P_R(F_\mathrm{R}) = \mathbf{M} \tag{10.26}$$

for any $J \in \mathbb{R}^{3\times 3}$ symmetric, where $\mathbf{M} \in \mathbb{R}^3$ is the torque vector applied to the object, given in the object reference frame e.

The proof of Proposition 1 is presented in the Appendix. As a direct consequence of (Eq. 10.25) and (10.26), the rotational dynamics of the body are given by:

$$2P_R\left(\frac{\mathrm{d}}{\mathrm{d}t}\nabla_{\dot{R}}\mathscr{L} - \nabla_R\mathscr{L}\right) = J\dot{\omega} + \omega\times J\omega + 2P_R\left(\nabla_R \nu^T c(\mathbf{q}, R)\right) = \mathbf{M}. \tag{10.27}$$

The translational dynamics are trivially obtained from (Eq. 10.18), and read:

$$m\ddot{\mathbf{r}} - \nabla_\mathbf{r}\mathscr{L} = \mathbf{F} \tag{10.28}$$

Using (Eq. 10.4), the index reduction on $q = \{\mathbf{r}, R\}$ for constraint i reads:

$$\begin{aligned}\dot{c}_i &= \nabla_{\mathbf{r}} c_i^T \dot{\mathbf{r}} + \mathrm{tr}\left(\nabla_R c_i^T \dot{R}\right) = \nabla_{\mathbf{r}} c_i^T \dot{\mathbf{r}} + \mathrm{tr}\left(\nabla_R c_i^T R \omega_\times\right) \\ &= \nabla_{\mathbf{r}} c_i^T \dot{\mathbf{r}} - 2U\left(\nabla_R c_i^T R\right)^T \omega = \nabla_{\mathbf{r}} c_i^T \dot{\mathbf{r}} + 2P_R\left(\nabla_R c_i\right)^T \omega, \\ \ddot{c}_i &= \nabla_{\mathbf{r}} c_i^T \ddot{\mathbf{r}} + 2P_R\left(\nabla_R c_i\right)^T \dot{\omega} + \nabla_{\mathbf{r}} \dot{c}_i^T \dot{\mathbf{r}} + \mathrm{tr}\left(\nabla_R \dot{c}_i \dot{R}\right) \\ &= \nabla_{\mathbf{r}} c_i^T \ddot{\mathbf{r}} + 2P_R\left(\nabla_R c_i\right)^T \dot{\omega} + \nabla_{\dot{\mathbf{r}}} \dot{c}_i^T \dot{\mathbf{r}} + 2P_R\left(\nabla_R \dot{c}_i\right)^T \omega,\end{aligned} \tag{10.29}$$

hence, exploiting the linearity of the ∇ and P_R operators, the dynamics take the implicit form:

$$\begin{bmatrix} m & 0 & \nabla_{\mathbf{r}} c \\ 0 & J & 2P_R\left(\nabla_R c\right) \\ \nabla_{\mathbf{r}} c^T & 2P_R\left(\nabla_R c\right)^T & 0 \end{bmatrix} \begin{bmatrix} \ddot{\mathbf{r}} \\ \dot{\omega} \\ \nu \end{bmatrix} = \begin{bmatrix} \mathbf{F} + \nabla_{\mathbf{r}} \mathscr{L} \\ \mathbf{M} - \omega \times J\omega \\ -\nabla_{\mathbf{r}} \dot{c}^T \dot{\mathbf{r}} - 2P_R\left(\nabla_R \dot{c}\right)^T \omega \end{bmatrix}, \tag{10.30}$$

where the following short notations are used:

$$P_R\left(\nabla_R c\right) = \left[P_R\left(\nabla_R c_1\right) \ldots P_R\left(\nabla_R c_{n_c}\right)\right], \quad P_R\left(\nabla_R \dot{c}\right) = \left[P_R\left(\nabla_R \dot{c}_1\right) \ldots P_R\left(\nabla_R \dot{c}_{n_c}\right)\right]$$

The consistency conditions:

$$c\left(\mathbf{r}(t_0), R(t_0)\right) = 0, \quad \dot{c}\left(\mathbf{r}(t_0), R(t_0)\right) = 0, \quad R(t_0)^T R(t_0) - I = 0 \tag{10.31}$$

must be enforced at some time t_0 of the trajectory.

It is straightforward to compute the expressions $\nabla_{\mathbf{r}} \dot{c}$, $\nabla_{\mathbf{r}} c$, $P_R\left(\nabla_R \dot{c}\right)$, $P_R\left(\nabla_R c\right)$ in (Eq. 10.30) using a Computer Algebra System (CAS). For the sake of illustration, however, they will be computed explicitly in the following examples.

10.3 A Single Wing AWE System in Pumping Mode

This section presents a model of a single-wing AWE system (see Fig. 10.1, right, for a schematic). The tether is considered as a rigid link of varying length l. The tether acceleration $\ddot{L}$ is a control variable. For the sake of simplicity, it is assumed here that the relative variation of the tether length is small, such that the tether mass is considered constant. The tether attachment point to the wing, given in the wing reference frame e is given by the vector $\mathbf{r}_{\mathrm{T}} \in \mathbb{R}^3$. The single constraint reads:

$$c(\mathbf{r}, R, L) = \frac{1}{2}\left(\left(\mathbf{r} + R\mathbf{r}_{\mathrm{T}}\right)^T \left(\mathbf{r} + R\mathbf{r}_{\mathrm{T}}\right) - l^2\right) = 0, \tag{10.32}$$

so that the attachment point of the tether to the aircraft is always at a distance l from the origin. It follows that:

$$\begin{aligned} 2P_R\left(\nabla_R c\right) = 2P_R\left(\nabla_R\left(\mathbf{r}^T R\mathbf{r}_{\mathrm{T}}\right)\right) = 2P_R\left(\mathbf{r}\mathbf{r}_{\mathrm{T}}^T\right) = 2U\left(R^T \mathbf{r}\mathbf{r}_{\mathrm{T}}^T\right) = \mathbf{r}_{\mathrm{T}} \times R^T \mathbf{r}, \\ \nabla_{\mathbf{r}} c = \mathbf{r} + R\mathbf{r}_{\mathrm{T}}. \end{aligned} \tag{10.33}$$

The kinetic and potential energy of the tether-wing system read:

$$T = \frac{1}{2}\left(m_{\mathrm{W}} + \frac{1}{3}m_{\mathrm{T}}\right)\dot{\mathbf{r}}^T\dot{\mathbf{r}} + \frac{1}{2}\boldsymbol{\omega}^T J\boldsymbol{\omega}, \qquad V = \left(m_{\mathrm{W}} + \frac{1}{2}m_{\mathrm{T}}\right)gz \tag{10.34}$$

where m_{W} is the mass of the wing and m_{T} is the mass of the tether, and J the matrix representation of the inertia tensor of the wing in the wing reference frame e. Using (Eq. 10.30) the system dynamics then read:

$$\begin{bmatrix} \left(m_{\mathrm{W}} + \frac{1}{3}m_{\mathrm{T}}\right)I_3 & 0 & \mathbf{r} + R\mathbf{r}_{\mathrm{T}} \\ 0 & J & \mathbf{r}_{\mathrm{T}} \times R^T\mathbf{r} \\ (\mathbf{r} + R\mathbf{r}_{\mathrm{T}})^T & (\mathbf{r}_{\mathrm{T}} \times R^T\mathbf{r})^T & 0 \end{bmatrix} \begin{bmatrix} \ddot{\mathbf{r}} \\ \dot{\boldsymbol{\omega}} \\ \nu \end{bmatrix} = \tag{10.35}$$

$$= \begin{bmatrix} \mathbf{F} - \left(m_{\mathrm{W}} + \frac{1}{2}m_{\mathrm{T}}\right)g\mathbf{1}_3 \\ \mathbf{M} - \boldsymbol{\omega} \times J\boldsymbol{\omega} \\ -\nabla_{\mathbf{r}}\dot{c}^T\dot{\mathbf{r}} - 2P_R\left(\nabla_R\dot{c}\right)^T\boldsymbol{\omega} + \dot{l}^2 + l\ddot{l} \end{bmatrix}. \tag{10.36}$$

where

$$\nabla_{\mathbf{r}}\dot{c} = \dot{\mathbf{r}} + R\left(\boldsymbol{\omega} \times \mathbf{r}_{\mathrm{T}}\right) \tag{10.37}$$

$$2P_R\left(\nabla_R\dot{c}\right) = 2P_R\left(\mathbf{r}\left(\boldsymbol{\omega} \times \mathbf{r}_{\mathrm{T}}\right)^T + \dot{\mathbf{r}}\mathbf{r}_{\mathrm{T}}^T\right) = -\left(R^T\mathbf{r}\right) \times \left(\boldsymbol{\omega} \times \mathbf{r}_{\mathrm{T}}\right) - \left(R^T\dot{\mathbf{r}}\right) \times \mathbf{r}_{\mathrm{T}}$$

In addition, the invariants (Eq. 10.32) and

$$\dot{c}\left(\mathbf{r}, \dot{\mathbf{r}}, R, \boldsymbol{\omega}, l, \dot{l}\right) = \left(\left(\mathbf{r} + R\mathbf{r}_{\mathrm{T}}\right)^T\left(\dot{\mathbf{r}} + R\left(\boldsymbol{\omega} \times \mathbf{r}_{\mathrm{T}}\right)\right) - l\dot{l}\right) = 0 \qquad R^TR - I = 0 \tag{10.38}$$

must be enforced at some time of the trajectory. Note that if the tether is attached at the center of mass of the wing, then $\mathbf{r}_{\mathrm{T}} = 0$, and $c(\mathbf{r}, R) = \frac{1}{2}\left(\mathbf{r}^T\mathbf{r} - l^2\right) = 0$. The dynamics then reduce to:

$$\begin{bmatrix} \left(m_{\mathrm{W}} + \frac{1}{3}m_{\mathrm{T}}\right)I_3 & 0 & \mathbf{r} \\ 0 & J & 0 \\ \mathbf{r}^T & 0 & 0 \end{bmatrix} \begin{bmatrix} \ddot{\mathbf{r}} \\ \dot{\boldsymbol{\omega}} \\ \nu \end{bmatrix} = \begin{bmatrix} \mathbf{F} - \left(m_{\mathrm{W}} + \frac{1}{2}m_{\mathrm{T}}\right)g\mathbf{1}_3 \\ \mathbf{M} - \boldsymbol{\omega} \times J\boldsymbol{\omega} \\ -\dot{\mathbf{r}}^T\dot{\mathbf{r}} + \dot{l}^2 + l\ddot{l} \end{bmatrix}. \tag{10.39}$$

10.3.1 Aerodynamics

This section proposes a model of the interaction of the wing with the air mass, using the DCM formulation. We define the wing relative velocity in the fixed frame E:

$$\mathbf{v} = \dot{\mathbf{r}} - \mathbf{w}(\mathbf{r}, t) \tag{10.40}$$

where $\mathbf{w}$ is the local wind velocity vector in e. The relative velocities in the wing reference frame e are then simply given by $\mathbf{V} = R^T\mathbf{v}$, such that the angle of attack (AoA) α and side-slip angle β read:

$$\alpha = -\tan\left(\frac{\mathbf{V}_z}{\mathbf{V}_\mathbf{x}}\right) = -\tan\left(\frac{\mathbf{e}_3^T\mathbf{v}}{\mathbf{e}_1^T\mathbf{v}}\right) \approx -\frac{\mathbf{e}_3^T\mathbf{v}}{\mathbf{e}_1^T\mathbf{v}}, \tag{10.41}$$

$$\beta = \tan\left(\frac{\mathbf{V}_y}{\mathbf{V}_\mathbf{x}}\right) = \tan\left(\frac{\mathbf{e}_2^T\mathbf{v}}{\mathbf{e}_1^T\mathbf{v}}\right) \approx \frac{\mathbf{e}_2^T\mathbf{v}}{\mathbf{e}_1^T\mathbf{v}}. \tag{10.42}$$

Constraints on the aerodynamic angles then reduce to quadratic expressions. E.g. a constraint on the maximal admissible value for α, can be formulated as:

$$\alpha \leq \alpha_{\max} \quad \leftrightarrow \quad (\alpha_{\max}\mathbf{e}_1 + \mathbf{e}_3)^T\,\mathbf{v} \geq 0 \tag{10.43}$$

The aerodynamic forces and moments F_A and T_A are then computed based on a coefficient-based aerodynamic model. The aerodynamic forces F_A and moments T_A read:

$$\mathbf{F}_\mathrm{A} = \frac{1}{2}\rho A\|\mathbf{v}\|(\underbrace{C_\mathrm{L}\mathbf{v}\times\mathbf{e}_2}_{\text{lift}} - \underbrace{C_\mathrm{D}\mathbf{v}}_{\text{drag}}), \quad \mathbf{M}_\mathrm{A} = \frac{1}{2}\rho A\|\mathbf{v}\|^2\begin{bmatrix} C_\mathrm{R} \\ C_\mathrm{P} \\ C_\mathrm{Y}\end{bmatrix}, \tag{10.44}$$

where the coefficients C_L, C_D, C_R, C_P, C_Y are functions of α, β, and ω. It can be observed that the velocity at any point on the tether is readily given by:

$$\mathbf{v} = \gamma\dot{\mathbf{r}} - \mathbf{w}(\gamma\mathbf{r}, t) \tag{10.45}$$

where $\gamma \in [0,1]$ spans the tether length. The contribution of the tether to the drag of the system can then be added in a finite element approach.

10.4 A Dual-wing AWE System in Drag Mode

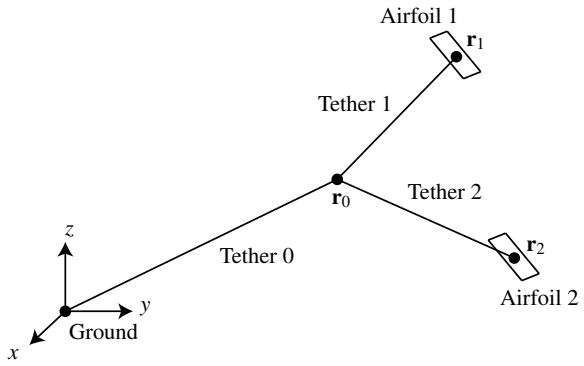

Fig. 10.3 Dual kite architecture

This section presents the model of a dual-wing AWE system, where two wings are attached via secondary tethers to a main tether (see Fig. 10.3). Such an architecture, though more complex, is known to reduce the tether drag, and improve the system performance (see e.g. [20]). The architecture yields three constraints:

$$c_0(\mathbf{r}_0, l_0) = \frac{1}{2}\left(\mathbf{r}_0^T\mathbf{r}_0 - l_0^2\right) = 0, \tag{10.46}$$

$$c_k(\mathbf{r}_k, R_k, l_k) = \frac{1}{2}\left(\left(\mathbf{r}_k + R_k\mathbf{r}_\mathrm{T} - \mathbf{r}_0\right)^T\left(\mathbf{r}_k + R_k\mathbf{r}_\mathrm{T} - \mathbf{r}_0\right) - l_k^2\right) = 0, \quad k = 1,2. \tag{10.47}$$

In natural coordinates, the kinetic energy associated to a rigid tether with extreme points a and b is given by:

$$T_\mathrm{tether} = \frac{1}{2}\mu L\int_0^1 \left((1-\zeta)\dot{\mathbf{r}}_a + \zeta\dot{\mathbf{r}}_b\right)^2 d\zeta = \frac{1}{6}\mu l\left(\dot{\mathbf{r}}_a^2 + \dot{\mathbf{r}}_b^2 + \dot{\mathbf{r}}_a\dot{\mathbf{r}}_b\right), \tag{10.48}$$

where μ is the tether linear mass and l its length.

The Lagrange function for the dual-wing AWE system then reads:

$$T = \underbrace{\frac{1}{6}\mu_0 l_0\dot{\mathbf{r}}_0^T\dot{\mathbf{r}}_0}_{\text{Main tether}} + \frac{1}{6}\sum_{k=1}^{2}\underbrace{\mu_k l_k\left(\dot{\mathbf{r}}_0^T\dot{\mathbf{r}}_0 + \dot{\mathbf{r}}_k^T\dot{\mathbf{r}}_k + \dot{\mathbf{r}}_0^T\dot{\mathbf{r}}_k\right)}_{\text{Secondary tether } k} + \underbrace{\sum_{k=1}^{2} m_k\dot{\mathbf{r}}_k^T\dot{\mathbf{r}}_k}_{\text{Wings, translation}} + \underbrace{\sum_{k=1}^{2} J_k\boldsymbol{\omega}_k^T\boldsymbol{\omega}_k}_{\text{Wings, rotation}} \tag{10.49}$$

$$V = \underbrace{\frac{1}{2}g\mu_0 l_0\mathbf{1}_3^T\mathbf{r}_0}_{\text{Main tether}} + \sum_{k=1}^{2}\underbrace{\frac{1}{2}g\mu_k l_k\mathbf{1}_3^T\left(\mathbf{r}_0 + \mathbf{r}_k\right)}_{\text{Secondary tether } k} + \underbrace{\sum_{k=1}^{2} g m_k\mathbf{1}_3^T\mathbf{r}_k}_{\text{Wings}} \tag{10.50}$$

so that, using $\xi_k = \frac{1}{3}\mu_k l_k I_3$, the dynamics read:

$$\begin{bmatrix} M & C \\ C^T & 0 \end{bmatrix}\begin{bmatrix} \ddot{\mathbf{r}} \\ \dot{\boldsymbol{\omega}} \\ \nu \end{bmatrix} = F, \qquad \ddot{\mathbf{r}} = \begin{bmatrix} \ddot{\mathbf{r}}_0 \\ \ddot{\mathbf{r}}_1 \\ \ddot{\mathbf{r}}_2 \end{bmatrix}, \quad \dot{\boldsymbol{\omega}} = \begin{bmatrix} \dot{\omega}_1 \\ \dot{\omega}_2 \end{bmatrix}, \quad \nu = \begin{bmatrix} \nu_0 \\ \nu_1 \\ \nu_2 \end{bmatrix} \tag{10.51}$$

where

$$M = \begin{bmatrix} \sum_{k=0}^{3}\xi_k & \frac{1}{2}\xi_1 & \frac{1}{2}\xi_2 & 0 & 0 \\ \frac{1}{2}\xi_1 & \xi_1 + m_1 I_3 & 0 & 0 & 0 \\ \frac{1}{2}\xi_2 & 0 & \xi_2 + m_2 I_3 & 0 & 0 \\ 0 & 0 & 0 & J_1 & 0 \\ 0 & 0 & 0 & 0 & J_2 \end{bmatrix}, \quad C = \begin{bmatrix} \mathbf{r}_0 & \nabla_{\mathbf{r}_0} c_1 & \nabla_{\mathbf{r}_0} c_2 \\ 0 & \nabla_{\mathbf{r}_1} c_1 & 0 \\ 0 & 0 & \nabla_{\mathbf{r}_2} c_2 \\ 0 & \Pi_1 & 0 \\ 0 & 0 & \Pi_2 \end{bmatrix},$$

$$F = \begin{bmatrix} \mathbf{F}_0 - \frac{1}{2} g \mu_0 l_0 \mathbf{1}_3 - \sum_{k=1}^{2} \frac{1}{2} g \mu_k l_k \mathbf{1}_3 \\ \mathbf{F}_1 - \frac{1}{2} g \mu_1 l_1 \mathbf{1}_3 - g m_1 \mathbf{1}_3 \\ \mathbf{F}_2 - \frac{1}{2} g \mu_2 l_2 \mathbf{1}_3 - g m_2 \mathbf{1}_3 \\ \mathbf{M}_1 - \omega_1 \times J_1 \omega_1 \\ \mathbf{M}_2 - \omega_2 \times J_2 \omega_2 \\ \nabla_{\mathbf{r}_0} \dot{c}_0^T \dot{\mathbf{r}}_0 \\ -\nabla_{\mathbf{r}_0} \dot{c}_1^T \dot{\mathbf{r}}_0 - \nabla_{\mathbf{r}_1} \dot{c}_1^T \dot{\mathbf{r}}_1 - 2 P_{R_1} \left(\nabla_{R_1} \dot{c}_1\right)^T \omega_1 \\ -\nabla_{\mathbf{r}_0} \dot{c}_2^T \dot{\mathbf{r}}_0 - \nabla_{\mathbf{r}_2} \dot{c}_2^T \dot{\mathbf{r}}_2 - 2 P_{R_2} \left(\nabla_{R_2} \dot{c}_2\right)^T \omega_2 \end{bmatrix} \tag{10.52}$$

with $\Pi_k = 2 P_{R_k}\left(\nabla_{R_k} c_k\right)$. Using the same development as in Eqns. (10.33) and (10.37), it can be verified that:

$$\dot{c}_0 = \mathbf{r}_0^T \dot{\mathbf{r}}_0, \qquad \dot{c}_k = \left(\mathbf{r}_k + R_k \mathbf{r}_{\mathrm{T}} - \mathbf{r}_0\right)^T \left(\dot{\mathbf{r}}_k + R_k \omega_k \times \mathbf{r}_{\mathrm{T}} - \dot{\mathbf{r}}_0\right) \tag{10.53}$$

$$\nabla_{\mathbf{r}_0} c_0 = \mathbf{r}_0, \quad -\nabla_{\mathbf{r}_0} \dot{c}_k = \nabla_{\mathbf{r}_k} \dot{c}_k = \left(\dot{\mathbf{r}}_k + R_k \omega_k \times \mathbf{r}_{\mathrm{T}} - \dot{\mathbf{r}}_0\right), \tag{10.54}$$

$$2 P_{R_k}\left(\nabla_{R_k} c_k\right) = \mathbf{r}_{\mathrm{T}} \times R_k^T \left(\mathbf{r}_k - \mathbf{r}_0\right), \quad -\nabla_{\mathbf{r}_0} c_k = \nabla_{\mathbf{r}_k} c_k = \mathbf{r}_k + R \mathbf{r}_{\mathrm{T}} - \mathbf{r}_0, \tag{10.55}$$

$$2 P_{R_k}\left(\nabla_{R_k} \dot{c}_k\right) = R^T \left(\mathbf{r} - \mathbf{r}_0\right) \times \left(\omega \times \mathbf{r}_{\mathrm{T}}\right) + R^T \left(\dot{\mathbf{r}} - \dot{\mathbf{r}}_0\right) \times \mathbf{r}_{\mathrm{T}}, \tag{10.56}$$

If the secondary tethers are attached to the center of mass of the wings, then:

$$P_{R_k}\left(\nabla_{R_k} c_k\right) = 0, \qquad P_{R_k}\left(\nabla_{R_k} \dot{c}_k\right) = 0 \tag{10.57}$$

In addition to the dynamics (Eq. 10.51), the invariants

$$c_k = 0, \quad \dot{c}_k = 0, \quad k = 0, 1, 2 \qquad \text{and} \qquad R^T R - I = 0 \tag{10.58}$$

must be enforced at some point of the trajectory.

10.5 Rotational Startup

A model for the rotational startup can be easily developed in the framework presented in Sect. 10.2, following a similar approach to Sect. 10.3 and 10.4. However, a major drawback of choosing an inertial reference frame for the carousel startup is that, even if the wing is at steady-state with respect to the carousel, the coordinates x,y,z and the rotation matrix R undergo periodic cycles at the frequency of the carousel, which costs useless computational burden for the integrator. To tackle that issue, this section presents an extension of the proposed modeling approach to a non-inertial (i.e. moving) reference frame attached to the carousel (see Fig. 10.4).

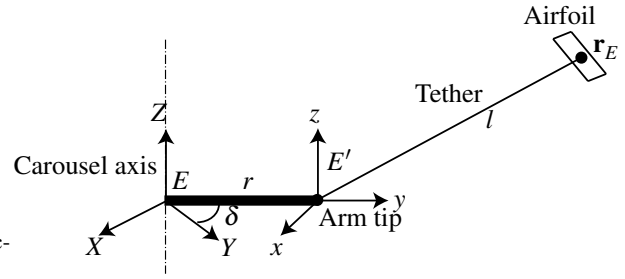

Fig. 10.4 Carousel architecture

In the following, the generalized coordinates $\mathbf{r} = [x\ y\ z]^T$ denote the position of the wing with respect to the moving frame E', while $\mathbf{r}_E$ denotes the position of the wing in the inertial (fixed) reference frame E. The single constraint reads:

$$c(\mathbf{r}, R, l) = \frac{1}{2}\left((\mathbf{r} + R\mathbf{r}_\mathrm{T})^T(\mathbf{r} + R\mathbf{r}_\mathrm{T}) - l^2\right) = 0. \tag{10.59}$$

where $\mathbf{r}_\mathrm{T} \in \mathbb{R}^3$ is the tether attachment point to the wing, given in the wing reference frame e. Assuming that the tether is massless, the kinetic and potential energy are given by:

$$T = \frac{1}{2}J_\mathrm{c}\dot{\delta}^2 + \frac{1}{2}m\dot{\mathbf{r}}_E^T\dot{\mathbf{r}}_E + \frac{1}{2}\omega^T J\omega \quad \text{and} \quad V = mgz \tag{10.60}$$

where J_c is the inertia of the carousel (excluding the plane) and

$$\mathbf{r}_E = R_\delta\left(\begin{bmatrix} r+x \\ y \\ z \end{bmatrix}\right), \qquad R_\delta = \begin{bmatrix} \cos\delta & -\sin\delta & 0 \\ \sin\delta & \cos\delta & 0 \\ 0 & 0 & 1 \end{bmatrix} \tag{10.61}$$

and ω is the angular velocity vector between the inertial reference frame and the wing, given in the wing reference frame. The time derivative of the rotation matrix R is given by:

$$\dot{R} = R\tilde{\omega}_\times \tag{10.62}$$

where $\tilde{\omega} = \omega - R^T\mathbf{1}_z\dot{\delta}$ is the angular velocity between the aircraft and the carousel frames, given in the aircraft frame, so that

$$\omega = P_R(\dot{R}) + R^T\mathbf{1}_z\dot{\delta}. \tag{10.63}$$

It can be verified that the results presented in Sect. 10.2.2 are equally valid, i.e. (Eq. 10.27) holds. For the sake of brevity this will not be established here.

Because of the choice of a non-inertial reference frame, however, the dynamics associated to the translations and carousel rotation will include coriolis terms. Using $\xi^T = \begin{bmatrix}\delta & q^T\end{bmatrix}$, the translational and carousel dynamics are given by:

$$\frac{d}{dt}\nabla_{\dot{\xi}}\mathscr{L} - \nabla_{\xi}\mathscr{L} = \frac{d}{dt}\nabla_{\dot{\xi}}T - \nabla_{\xi}\left(T-V\right) + \nabla_{\xi}\left(\nu^T c(\mathbf{r},R,l)\right) = F_{\xi} \tag{10.64}$$

where $\frac{d}{dt}\nabla_{\dot{\xi}}T = M\ddot{\xi} + C\dot{\xi}$, with:

$$M = \nabla_{\dot{\xi}\dot{\xi}}\left(\tfrac{1}{2}J_{\mathrm{c}}\dot{\delta}^2 + \tfrac{1}{2}m\dot{\mathbf{r}}_E^T\dot{\mathbf{r}}_E\right), \qquad C = \nabla_{\dot{\xi}\xi}\left(\tfrac{1}{2}J_{\mathrm{c}}\dot{\delta}^2 + \tfrac{1}{2}m\dot{\mathbf{r}}_E^T\dot{\mathbf{r}}_E\right) \tag{10.65}$$

The *generalized inertia matrix M* and the *coriolis matrix C* can be easily extracted using a CAS, but are not displayed here for sake of brevity. Following a similar development as in (Eq. 10.29), it can be verified that:

$$\dot{c} = \nabla_{\xi}c^T\dot{\xi} + 2P_R\left(\nabla_R c\right)^T\left(\omega - R^T\mathbf{1}_z\dot{\delta}\right) - l\dot{l} \tag{10.66}$$

$$\begin{aligned}\ddot{c} = \nabla_{\xi}c^T\ddot{\xi} + 2P_R\left(\nabla_R c\right)^T\left(\dot{\omega} - R^T\mathbf{1}_z\ddot{\delta}\right) + \nabla_{\xi}\dot{c}^T\dot{\xi} \\ + 2P_R\left(\nabla_R\dot{c}\right)^T\left(\omega - R^T\mathbf{1}_z\dot{\delta}\right) - l\ddot{l} - \dot{l}^2\end{aligned} \tag{10.67}$$

hence

$$\begin{aligned}\ddot{c} = \left(\nabla_{\xi}c^T - 2P_R\left(\nabla_R c\right)^T R^T\mathbf{I}_z\right)\ddot{\xi} + 2P_R\left(\nabla_R c\right)^T\dot{\omega} \\ + \nabla_{\xi}\dot{c}^T\dot{\xi} + 2P_R\left(\nabla_R\dot{c}\right)^T\left(\omega - R^T\mathbf{1}_z\dot{\delta}\right)\end{aligned} \tag{10.68}$$

where

$$\mathbf{I}_z = \begin{bmatrix}0&0&0&0\\0&0&0&0\\1&0&0&0\end{bmatrix}$$

and $2P_R\left(\nabla_R c\right)$ and $2P_R\left(\nabla_R\dot{c}\right)$ are given by Eqns. (10.33) and (10.37), and

$$\nabla_{\xi}c = \begin{bmatrix}0\\ \mathbf{r}_{\mathrm{T}} \times R^T\mathbf{r}\end{bmatrix} \tag{10.69}$$

As a result, the index-reduced dynamics read

$$\begin{bmatrix} M & \mathbf{0} & \nabla_{\xi}c \\ \mathbf{0} & J & \mathbf{r}_{\mathrm{T}}\times R^T\mathbf{r} \\ \nabla_{\xi}c^T - \left(\mathbf{r}_{\mathrm{T}}\times R^T\mathbf{r}\right)^T R^T\mathbf{I}_z & \left(\mathbf{r}_{\mathrm{T}}\times R^T\mathbf{r}\right)^T & 0\end{bmatrix}\begin{bmatrix}\ddot{\xi}\\ \dot{\omega}\\ \nu\end{bmatrix} = \begin{bmatrix} F_{\xi} - C\dot{\xi} + \nabla_{\xi}\left(T-V\right) \\ \mathbf{M} - \omega\times J\omega \\ -\nabla_{\xi}\dot{c}^T\dot{\xi} - 2P\left(\nabla_R\dot{c}\right)^T\left(\omega - R^T\mathbf{1}_z\dot{\delta}\right) + \dot{l}^2 + l\ddot{l}\end{bmatrix} \tag{10.70}$$

It can be observed that the choice of coordinates, where $\dot{R}$ is a function of both ω and $\dot{\delta}$, destroys the symmetry of the right-hand-side matrix in (10.70).

10.6 Stabilization of the constraints

In natural coordinates, the over-parametrized representation of the system is meaningful only if the set of coordinates are initiated on a manifold yielded by the index-reduction. In the case presented here, the manifold is given by Eq. 10.31.

Due to the inaccuracy of numerical integration [14], however, the natural coordinates will tend to drift away from the manifold over time. The numerical drift is not a problem in the framework of Model Predictive Control [8], where the system is typically simulated over reasonably short periods of time. For long simulation, however, the numerical drift must be addressed.

Because the second-order time derivative of $c(\mathbf{r},R)$, i.e. $\ddot{c}(\mathbf{r},R)$, is simply set to zero by the index-reduced model equations (Eq. 10.30), the dynamics of $c(\mathbf{r},R)$ are unstable. The dynamics of $c(\mathbf{r},R)$ can be stabilized by replacing $\ddot{c}(\mathbf{r},R)=0$ by:

$$\ddot{c}(\mathbf{r},R) = -2\kappa\dot{c}(\mathbf{r},R) - \kappa^2 c(\mathbf{r},R), \tag{10.71}$$

in (Eq. 10.29), where $\kappa > 0$ provides the time constant of the stabilized dynamics. The right-hand-side of the dynamics (Eq. 10.30) are therefore modified to:

$$\begin{bmatrix} \mathbf{F} + \nabla_{\mathbf{r}}\mathscr{L} \\ \mathbf{M} - \boldsymbol{\omega} \times J\boldsymbol{\omega} \\ -\nabla_{\mathbf{r}}\dot{c}^T\dot{\mathbf{r}} - 2P_R\left(\nabla_R\dot{c}\right)^T\boldsymbol{\omega} - 2\kappa\dot{c}(\mathbf{r},R) - \kappa^2 c(\mathbf{r},R) \end{bmatrix}. \tag{10.72}$$

The orthonormality of the rotation matrix R can be stabilized by modifying the dynamics (Eq. 10.15) of R to:

$$\dot{R} = R\left(\boldsymbol{\omega}_\times + \Xi\right), \tag{10.73}$$

with $\Xi = \frac{\kappa}{2}\left(\left(R^TR\right)^{-1} - I\right)$ skew symetric, it can be verified that:

$$\frac{d}{dt}\left(R^TR - I\right) = -\kappa\left(R^TR - I\right). \tag{10.74}$$

and the orthonormality condition is stabilized for any $\kappa > 0$. See [8] for further details.

10.7 Illustrative simulation

As an illustration, a simulation using the carousel model (10.70) was performed. The aerodynamic forces were computed using the aerodynamic model used in [9]. The dynamics (10.70) were integrated using a Runge-Kutta 4/5 scheme. The DAE (10.70) was treated as an explicit ODE using a numerical back-solve inversion of the mass matrix. The simulation was started at steady-state, with a tether length l of

1.2 [m]. The tether was then extended to a length of 5 [m], with neutral control surfaces and constant carousel torque. Fig. 10.7 displays the resulting carousel angular velocity $\dot{\delta}$ and the tether length l. Fig. 10.5 displays the resulting 3D trajectories in the reference frame attached to the carousel arm tip. Fig. 10.7 displays the resulting x, y, z trajectories, with the tether force. Fig. 10.7 displays the trajectory of the constraint c and its time derivatives $\dot{c}$, $\ddot{c}$ over the simulation time.

It can be observed in Fig. 10.7 that the constraint drifts away over time, and can corrected by a stabilization of the constraints numerical drift, as discussed in Sect. 10.6.

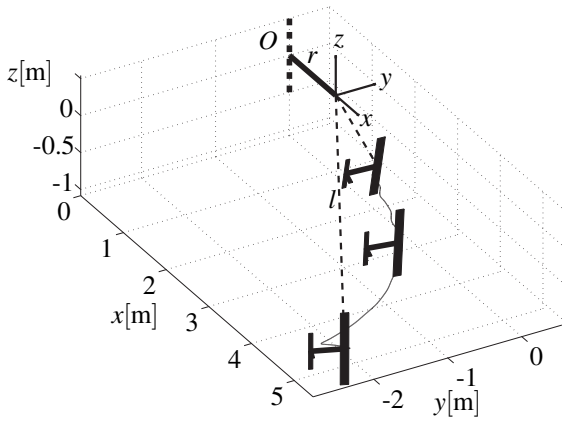

Fig. 10.5 Carousel 3D Trajectory in the carousel frame E'. The xyz-frame rotates with the carousel, hence the reported trajectory is relative to the carousel arm. The thin dashed lines indicate the tether position at the beginning and the end of the simulation. The plain, thin curve represents the center of mass the trajectory of the plane.

10.8 Minimal versus Natural Coordinates: a Case Study

This section presents a case study to support the claim made in the introduction that the natural coordinate approach can offer a clear-cut advantage over the minimal coordinate approach by reducing the computational complexity and nonlinearity. To that end, the dual-kite AWE system in drag mode is modeled using both:

1. the natural coordinate approach presented in Sect. 10.4. The resulting model is an index-1 DAE in the form (Eq. 10.51).
2. a minimal coordinate approach, using azimuth and elevation angles for the three tethers and Euler angles for the two kites, resulting in an implicit ODE model in the form:

$$M(\mathbf{q}, \dot{\mathbf{q}})\,\ddot{\mathbf{q}} - \mathbf{G}(\mathbf{q}, \dot{\mathbf{q}}) = 0, \tag{10.75}$$

where $M \in \mathbb{R}^{12\times 12}$ is the generalized inertia matrix, $\mathbf{G} \in \mathbb{R}^{12}$ the vector of equivalent generalized forces (including the pseudo-forces resulting from inertial effects), and

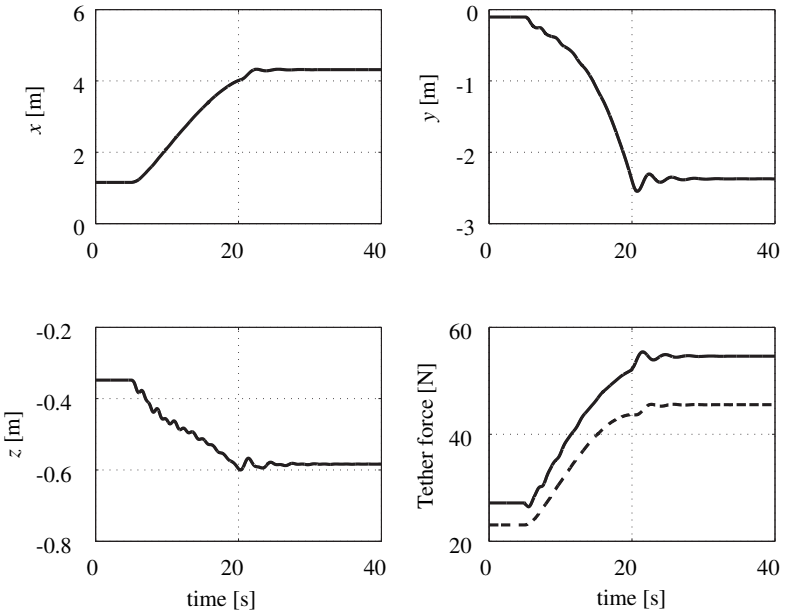

Fig. 10.6 Carousel x,y,z trajectory and tether force. The dashed line in the lower-right graph reports the magnitude of the force due to the combination of the centrifugal accelerations and gravity when the plane is a steady state, computed using the formula $m\|[(r+x)\dot{\delta}^2 \quad 0 \quad -g]\|$. It can be observed that the tether force and the force due to the plane acceleration are of the same order of magnitude (note that the two forces are not supposed to match, since the forces compared are not collinear vectors, and a difference is introduced by the aerodynamic forces).

$$\mathbf{q} = \begin{bmatrix} \phi_0 & \psi_0 & \phi_1 & \psi_1 & \alpha_1 & \beta_1 & \gamma_1 & \phi_2 & \psi_2 & \alpha_2 & \beta_2 & \gamma_2 \end{bmatrix}^T \in \mathbb{R}^{12}$$

where ϕ_i, ψ_i are the azimuth and elevation angles of tether $i = 0,1,2$ with respect to the downwind direction and α_k, β_k, γ_k are the Euler angles describing the orientation of kite $k = 1,2$ using the rotation sequence $1-2-3$ of the inertial reference frame.

Note that the symbolic inversion of the generalized inertia matrix M is overly costly and should not be attempted, hence the model equations must be considered in their implicit form (Eq. 10.75). For further details on the modeling of multiple-kite AWE systems in minimal coordinates, the reader is referred to e.g. [18].

It was considered here that the secondary tethers are attached directly to the center of mass of the kite. Both models have been developed in the Lagrangian formalism, using the Computer Algebra System *Mupad*. The graph representations, and Automatic Differentiation (AD) for the two models has been performed using the AD tool *CasADi* [1].

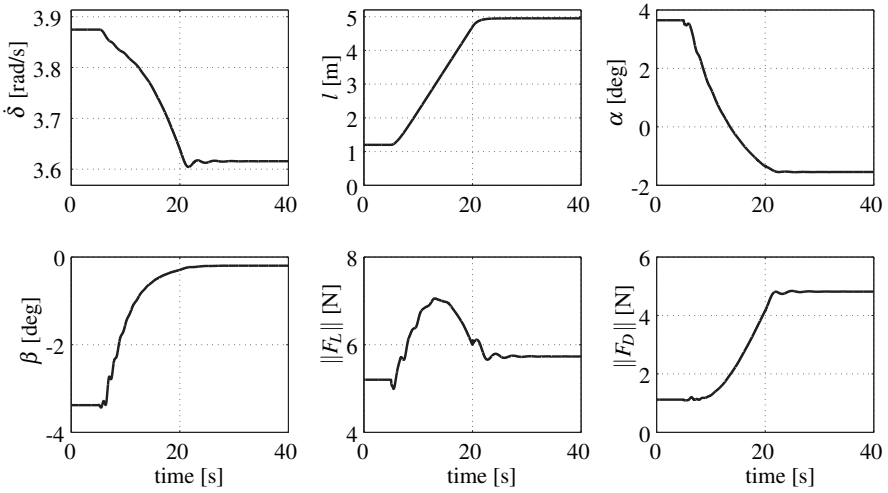

Fig. 10.7 Carousel velocity $\dot{\delta}$, tether length l, angle of attack α, side-slip angle β, norm of the lift force F_{L} and of the drag force F_{D}. As the tether length is extended, the plane tends to pitch down, hence the lifting force and drag increase only moderately. In this simulation, the carousel velocity decreases only slightly, because the friction parameter was chosen rather large, hence the influence of the plane to the carousel velocity is mild.

10.8.1 Model Complexity and Cost of Evaluation

The comparison of the two modeling approaches was based on the model equations (Eq. 10.51) versus (Eq. 10.75), their sensitivities with respect to all variables (hereafter labeled *Jacobian*), and the derivative of their directional sensitivities with respect to all variables (hereafter labeled *Hessian*, by a slight abuse of language)

These three functions need to be evaluated at each step of exact Newton schemes. The comparison proposed here considers for each of these three functions a) the number of nodes in their graph representations, providing a measure of their symbolic complexity, and b) the typical computational time required for their evaluation. A gain in computational time entails a corresponding speed increase of sensitivity-based optimization techniques. The comparison is reported in table 10.1, with the caveat that the computational times and ratios are characteristic but can vary depending on the CPU and the C compiler used.

It can be observed that the natural coordinate approach results in a significant reduction of the complexity and cost-of-evaluation of the model equations, Jacobian and Hessian of the system.

The same comparison has been carried out by introducing in both models the high-fidelity model of the aerodynamic forces presented e.g. [7], which follows the lines of Sect. 10.3.1. The comparison is reported in table 10.2. It can be observed that even with the introduction of a complex aerodynamic model, the advantage of

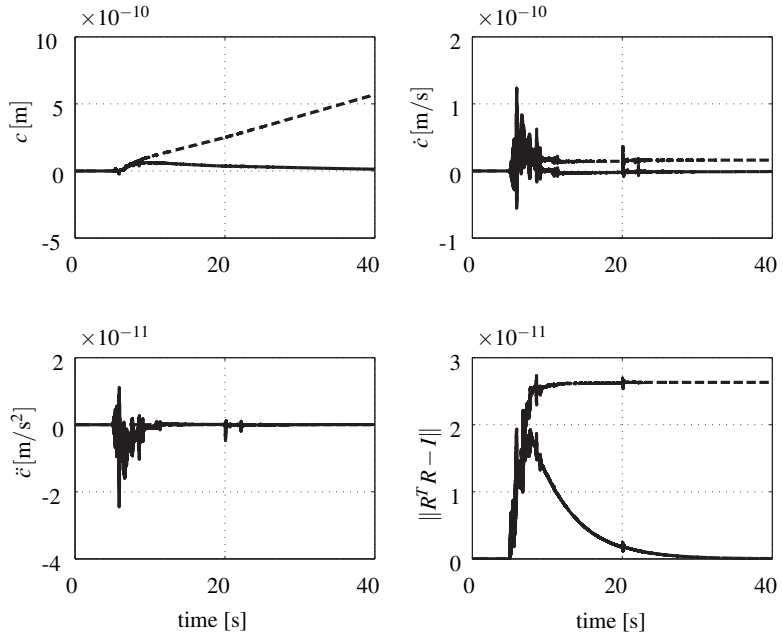

Fig. 10.8 Trajectory of the constraint c, its time derivatives $\dot{c}$, $\ddot{c}$, and norm of the $SO(3)$ constraint error, without constraint stabilization (dashed line), and with constraint stabilization (plain line), using a stabilization parameter $\kappa = 0.1\,\mathrm{s}^{-1}$. See Sect. 10.6 for the details of constraint stabilization.

Table 10.1 Model comparison without aerodynamic forces, the computational times are reported in μs, averaged over 10^4 function evaluations.

Model type	model: #nodes / time	Jacobian: #nodes / time	Hessian: #nodes / time
Natural	372 / 9.8	237 / 9.7	206 / 9.2
Minimal	1068 / 13.9	3484 / 30.1	16092 / 107.7
Ratio Minimal/Natural	2.9 / 1.4	14.7 / 3.1	78.1 / 11.7

the natural coordinate approach remains significant.

10.9 Conclusion and Future Work

This paper has proposed a modeling technique for AWE systems that yields models of lower symbolic complexity, and lower nonlinearity than more conventional approaches. A case study has been proposed to show the reduction of symbolic

Table 10.2 Model comparison with aerodynamic forces, the computational times are reported in μs, averaged over 10^4 function evaluations.

Model type	model: #nodes / time	Jacobian: #nodes / time	Hessian: #nodes / time
Natural	615 / 10.6	1377 / 19.5	17516 / 122.2
Minimal	1794 / 18.4	9054 / 66.0	117823 / 745.7
Ratio Minimal/Natural	2.9 / 1.74	6.6 / 3.4	6.7 / 6.1

complexity. The reduction of the model symbolic complexity generally translates into a reduction of the cost of an evaluation of the model equations and its first and second-order sensitivities. The reduction of model nonlinearity has been observed in practice via the optimization of several AWE systems, showing that the convergence of Newton schemes is better when working in natural coordinates than in minimal coordinates. This observation deserves, however, more studies, and is the object of future work.

The proposed modeling approach is primarily aimed at providing models that are best suited for direct optimization, where a reduction of the model computational cost and nonlinearity yields a speed up in the convergence of Newton-type optimization techniques. If the model is developed for the sole purpose of simulations, the advantage of models based on natural coordinates can be less significant. A drawback of the proposed approach is its high level of abstraction, which may discourage regular users of AWE modeling. To alleviate that problem, an object-oriented modeling software for AWE system will be developed to manipulate the concepts proposed in this paper in a simple and intuitive way.

Several illustrative examples are proposed in this chapter: the modeling of a single wing in pumping mode, the modeling of a dual-wing system in drag mode, and the modeling of a rotational startup. In all cases, the offset between the tether attachment point and the center of mass of the wing is taken into account. A simulation of the experimental setup is available at KU Leuven (see Chap. 27), showing how the proposed modeling approach can be applied. The reader is referred to Chaps. 11 and 12 to see more applications of the proposed modeling approach in the framework of power optimization and control for AWE systems.

In future work, a differentiable model for tether dynamics of varying length will be included in the proposed modeling approach, so that it can be used in the optimization framework.

Acknowledgements This research was supported by Research Council KUL: PFV/10/002 Optimization in Engineering Center OPTEC, GOA/10/09 MaNet and GOA/10/11 Global real- time optimal control of autonomous robots and mechatronic systems. Flemish Government: IOF / KP / SCORES4CHEM, FWO: PhD/postdoc grants and projects: G.0320.08 (convex MPC), G.0377.09 (Mechatronics MPC); IWT: PhD Grants, projects: SBO LeCoPro; Belgian Federal Science Policy Office: IUAP P7 (DYSCO, Dynamical systems, control and optimization, 2012-2017); EU: FP7-EMBOCON (ICT-248940), FP7-SADCO (MC ITN-264735), ERC ST HIGHWIND (259 166), Eurostars SMART, ACCM.

10.10 Appendix

10.10.1 Some Properties of Operators P and U

It can be verified that the following equalities hold $\forall \mathbf{a},\mathbf{b} \in \mathbb{R}^3$ and $\forall R \in SO(3)$, $\dot{R}$ in the tangent space to $SO(3)$ at R:

$$\begin{aligned}
&\nabla_{\dot{R}}\left(P(\dot{R})^T\mathbf{a}\right) = \frac{1}{2}R\mathbf{a}_\times \qquad \nabla_R\left(P(\dot{R})^T\mathbf{a}\right) = -\frac{1}{2}\dot{R}\mathbf{a}_\times \\
&U\left(\mathbf{a}_\times\mathbf{b}_\times\right) = \quad \frac{1}{2}\mathbf{a}\times\mathbf{b} \qquad U\left(\mathbf{a}\mathbf{b}^T\right) = -\frac{1}{2}\mathbf{a}\times\mathbf{b} \\
&\nabla_R\left(\mathbf{a}^TR\mathbf{b}\right) = \mathbf{a}\mathbf{b}^T \qquad \mathrm{tr}\left(A\mathbf{a}_\times\right) = -2U(A)^T\mathbf{a} \\
&-U\left(A^TR\right) = P(A), \qquad \mathrm{tr}\left(\mathbf{a}_\times^TA\right) = 2\mathbf{a}^TU(A)
\end{aligned} \tag{10.76}$$

10.10.2 Proof of Proposition 1:

Consider

$$\nabla_{\dot{R}}\left(\frac{1}{2}\omega^TJ\omega\right) = \nabla_{\dot{R}}\left(P(\dot{R})^TJ\omega\right) = \frac{1}{2}R(J\omega)_\times \tag{10.77}$$

hence

$$\begin{aligned}
&2P_R\left(\frac{\mathrm{d}}{\mathrm{d}t}\nabla_{\dot{R}}\left(P(\dot{R})^TJ\omega\right)\right) = P_R\left(\frac{\mathrm{d}}{\mathrm{d}t}\left(R(J\omega)_\times\right)\right) = P_R\left(R\omega_\times(J\omega)_\times\right) \\
&+P_R\left(R(J\dot{\omega})_\times\right) = U\left(\omega_\times(J\omega)_\times\right) + U\left((J\dot{\omega})_\times\right) = \frac{1}{2}\omega\times J\omega + J\dot{\omega}
\end{aligned} \tag{10.78}$$

Moreover

$$\begin{aligned}
&2P_R\left(\nabla_R\left(\frac{1}{2}\omega^TJ\omega\right)\right) = 2P_R\left(\nabla_R\left(P_R(\dot{R})^TJ\omega\right)\right) = \\
&P_R\left(-\dot{R}(J\omega)_\times\right) = -U\left(R^T\dot{R}(J\omega)_\times\right) = U\left(\omega_\times(J\omega)_\times\right) = -\frac{1}{2}\omega\times J\omega
\end{aligned} \tag{10.79}$$

Using (10.77), (10.78) and (10.79), the first equality in (Eq. 10.26) follows. The virtual work δW resulting from a compatible infinitesimal perturbation δR of R under the generalized force F_R is given by $\delta W = \mathrm{tr}\left(\delta R^TF_\mathrm{R}\right)$. The differential δR is given by $\delta R = R\delta\mathbf{s}_\times$ where $\delta\mathbf{s} \in \mathbb{R}^3$ is the equivalent infinitesimal rotation vector. The virtual work δW is also given by $\delta W = \langle\delta\mathbf{s},\mathbf{M}\rangle$. It follows that $\forall\,\delta\mathbf{s}$:

$$\langle\delta\mathbf{s},\mathbf{M}\rangle = \mathrm{tr}\left(\delta R^TF_\mathrm{R}\right) = \mathrm{tr}\left(\delta\mathbf{s}_\times^TR^TF_\mathrm{R}\right) = 2\delta\mathbf{s}^TU(R^TF_R) = \langle\delta\mathbf{s},2P_R(F_R)\rangle \tag{10.80}$$

hence $2P_R(F_\mathrm{R}) = \mathbf{M}$.

References

1. Andersson, J., Åkesson, J., Diehl, M.: CasADi – A symbolic package for automatic differentiation and optimal control. In: Forth, S., Hovland, P., Phipps, E., Utke, J., Walther, A. (eds.) Recent Advances in Algorithmic Differentiation, Vol. 87, Lecture Notes in Computational Science and Engineering, pp. 297–307. Springer, Berlin (2012). doi: 10.1007/978-3-642-30023-3_27
2. Ascher, U. M., Petzold, L. R.: Computer Methods for Ordinary Differential Equations and Differential–Algebraic Equations. SIAM Press, Philadelphia (1998)
3. Canale, M., Fagiano, L., Milanese, M.: High Altitude Wind Energy Generation Using Controlled Power Kites. IEEE Transactions on Control Systems Technology **18**(2), 279–293 (2010). doi: 10.1109/TCST.2009.2017933
4. Fagiano, L., Milanese, M., Piga, D.: Optimization of airborne wind energy generators. International Journal of Robust and Nonlinear Control **22**(18), 2055–2083 (2011). doi: 10.1002/rnc.1808
5. Fagiano, L., Milanese, M., Piga, D.: High-altitude wind power generation. IEEE Transactions on Energy Conversion **25**(1), 168–180 (2010). doi: 10.1109/TEC.2009.2032582
6. Groot, S. G. C. de, Breukels, J., Schmehl, R., Ockels, W. J.: Modeling Kite Flight Dynamics Using a Multibody Reduction Approach. AIAA Journal of Guidance, Control and Dynamics **34**(6), 1671–1682 (2011). doi: 10.2514/1.52686
7. Gros, S., Zanon, M., Diehl, M.: Control of Airborne Wind Energy Systems Based on Nonlinear Model Predictive Control & Moving Horizon Estimation. In: Proceedings of the European Control Conference (ECC13), Zurich, Switzerland, 17–19 July 2013
8. Gros, S., Zanon, M., Vukov, M., Diehl, M.: Nonlinear MPC and MHE for Mechanical Multi-Body Systems with Application to Fast Tethered Airplanes. In: Proceedings of the 4th IFAC Nonlinear Model Predictive Control Conference, pp. 86–93, Leeuwenhorst, Netherlands, 23–27 Aug 2012. doi: 10.3182/20120823-5-NL-3013.00061
9. Gros, S., Ahmad, H., Geebelen, K., Swevers, J., Diehl, M.: In-flight Estimation of the Aerodynamic Roll Damping and Trim Angle for a Tethered Aircraft based on Multiple-shooting. In: Proceedings of the 16th IFAC Symposium on System Identification, pp. 1407–1412, Brussels, Belgium, 11–13 July 2012. doi: 10.3182/20120711-3-BE-2027.00342
10. Houska, B.: Robustness and Stability Optimization of Open-Loop Controlled Power Generating Kites. M.Sc.Thesis, Ruprecht-Karls-Universität, Heidelberg, 2007. http://www.kuleuven.be/optec/files/Houska2007a.pdf
11. Joshi, A. W.: Elements of Group Theory for Physicists. 4th ed. New Age International Publishers, New Delhi (1997)
12. Pantelides, C. C., Sargent, R. W. H., Vassiliadis, V. S.: Optimal control of multistage systems described by high-index differential-algebraic equations. In: Bulirsch, R., Kraft, D. (eds.) Computational Optimal Control, ISNM International Series of Numerical Mathematics Vol. 115, pp. 177–191. Birkhäuser, Basel (1994). doi: 10.1007/978-3-0348-8497-6_15
13. Papastavridis, J. G.: Analytical Mechanics. Oxford University Press, New York (2002)
14. Schulz, V. H., Bock, H. G., Steinbach, M. C.: Exploiting invariants in the numerical solution of multipoint boundary value problems for DAEs. SIAM Journal on Scientific Computing **19**(2), 440–467 (1998). doi: 10.1137/S1064827594261917
15. Shabana, A. A.: Dynamics of Multibody Systems. 3rd ed. Cambridge University Press, Cambridge (2005)
16. Terink, E. J., Breukels, J., Schmehl, R., Ockels, W. J.: Flight Dynamics and Stability of a Tethered Inflatable Kiteplane. AIAA Journal of Aircraft **48**(2), 503–513 (2011). doi: 10.2514/1.C031108
17. Williams, P., Lansdorp, B., Ockels, W. J.: Modeling and Control of a Kite on a Variable Length Flexible Inelastic Tether. AIAA Paper 2007-6705. In: Proceedings of the AIAA Modelling and Simulation Technologies Conference and Exhibit, Hilton Head, SC, USA, 20–23 Aug 2007. doi: 10.2514/6.2007-6705

18. Williams, P., Lansdorp, B., Ockels, W. J.: Nonlinear Control and Estimation of a Tethered Kite in Changing Wind Conditions. AIAA Journal of Guidance, Control and Dynamics **31**(3) (2008). doi: 10.2514/1.31604
19. Williams, P., Lansdorp, B., Ruiterkamp, R., Ockels, W.: Modeling, Simulation, and Testing of Surf Kites for Power Generation. AIAA Paper 2008-6693. In: Proceedings of the AIAA Modeling and Simulation Technologies Conference and Exhibit, Honolulu, HI, USA, 18–21 Aug 2008. doi: 10.2514/6.2008-6693
20. Zanon, M., Gros, S., Andersson, J., Diehl, M.: Airborne Wind Energy Based on Dual Airfoils. IEEE Transactions on Control Systems Technology **21**(4), 1215–1222 (2013). doi: 10.1109/TCST.2013.2257781